Dating groundwater with dissolved silica and CFC concentrations in crystalline aquifers

Jean Marçais, Alexandre Gauvain, Thierry Labasque, Benjamin W Abbott,
Gilles Pinay, Luc Aquilina, Francois Chabaux, Daniel Viville, Jean-Raynald
de Dreuzy

HAL Id: insu-01779877
https://insu.hal.science/insu-01779877

Submitted on 27 Apr 2018

Dating groundwater with dissolved silica and CFC concentrations in crystalline aquifers

Jean Marçais[†1,2], Alexandre Gauvain[2], Thierry Labasque[2], Benjamin W. Abbott[3], Gilles Pinay[4], Luc Aquilina[2], François Chabaux[5], Daniel Viville[5], Jean-Raynald de Dreuzy[2]

[1] *Agroparistech, 75005 Paris, France*

[2] *OSUR, Géosciences Rennes, CNRS, Université de Rennes 1, 35042 Rennes Cedex, France*

[3] *Brigham Young University, Provo, UT, United States*

[4] *RiverLy-Irstea, Lyon, 5 rue de la Doua, 69616 Villeurbanne cedex, France*

[5] *Laboratoire d'Hydrologie et de Géochimie de Strasbourg (LHyGeS), CNRS, Université de Strasbourg, 67084 Strasbourg Cedex, France*

Abstract

Estimating intermediate water residence times (a few years to a century) in shallow aquifers is critical to quantifying groundwater vulnerability to nutrient loading and estimating realistic recovery timelines. While intermediate groundwater residence times are currently determined with atmospheric tracers such as chlorofluorocarbons (CFCs), these analyses are costly and would benefit from other tracer approaches to compensate for the decreasing resolution of CFC methods in the 5-20 years range. In this context, we developed a framework to assess the capacity of dissolved silica (DSi) to inform residence times in shallow aquifers. We calibrated silicate weathering rates with CFCs from multiple wells in five crystalline aquifers in Brittany and in the Vosges Mountains (France). DSi and CFCs were complementary in determining apparent weathering reactions and residence time distributions (RTDs) in shallow aquifers.

† Corresponding author: jean.marcais@univ-rennes1.fr

22   Silicate weathering rates were surprisingly similar among Brittany aquifers, varying from

23   0.20 to 0.23 mg L^{-1} yr^{-1} with a coefficient of variation of 7%, except for the aquifer where

24   significant groundwater abstraction occurred, where we observed a weathering rate of 0.31

25   mg L^{-1} yr^{-1}. The silicate weathering rate was lower for the aquifer in the Vosges Mountains

26   (0.12 mg L^{-1} yr^{-1}), potentially due to differences in climate and anthropogenic solute loading.

27   Overall, these optimized silicate weathering rates are consistent with previously published

28   studies with similar apparent ages range. The consistency in silicate weathering rates suggests

29   that DSi could be a robust and cheap proxy of mean residence times for recent groundwater

30   (5-100 years) at the regional scale. This methodology could allow quantification of seasonal

31   groundwater contributions to streams, estimation of residence times in the unsaturated zone

32   and improve assessment of aquifer vulnerability to anthropogenic pollution.

1   Introduction

36   Human activity has fundamentally altered global nutrient cycles (Galloway et al.,

37   2008), polluting aquatic ecosystems and threatening human health and water security

38   (Spalding and Exner, 1993). It is widely held that anthropogenic loading of nitrogen has

39   exceeded planetary capacities, representing one of the most pressing environmental issues

40   (Rockstrom et al., 2009; Steffen et al., 2015). International, national, and regional initiatives

41   have been undertaken in the past several decades to reduce nitrogen loading, though

42   assessment of efficacy is difficult in complex natural systems with unknown and overlapping

43   memory effects (Jarvie, 2013; Jenny et al., 2016; Meter and Basu, 2017; Wilcock et al.,

44   2013). Estimating the recovery time of surface and groundwater ecosystems following

45   nitrogen pollution is key to quantifying effectiveness of changes in agricultural practices,

46   mitigation methods, and developing realistic timelines for meeting regulatory goals (Abbott et

47   al., 2018; Bouraoui and Grizzetti, 2011; Jasechko et al., 2017). Recovery time depends largely

48   on water and solute residence time in the surface and subsurface components of the

49   catchment. The majority of catchment transit time occurs in the subsurface, where water can

50   spend months to years in the soil or unsaturated zone (Meter et al., 2016; Sebilo et al., 2013),

51   and decades to centuries in near-surface aquifers (Bohlke and Denver, 1995; Kolbe et al.,

52   2016; Singleton et al., 2007; Visser et al., 2013). Because no single tracer can determine the

53   distribution of groundwater ages across these timescales, multi tracer approaches are

54   necessary for reliable groundwater dating (Abbott et al., 2016).

55   Several tracers are well suited to determine residence times for timescales relevant to

56   nutrient pollution, including $^3H/^3He$ and chlorofluorocarbons (CFCs), because the

57   atmospheric concentration of these gases were altered by human activity coincident with the

58   great acceleration of nutrient loading in the mid-1900s (Aquilina et al., 2012b; Cook and

59   Herczeg, 2000; Labasque et al., 2014; Steffen et al., 2015; Visser et al., 2014). However, CFC

60   methods now lack resolution in the 5-20 years range because their atmospheric concentrations

61   peaked around 1998 following their prohibition by the Kyoto Protocol (**Figure 1**). This

62   reversal of atmospheric trends means any measured concentration between 1995 and 2018

63   corresponds to two dates. Additionally, 3H/3He and CFC samples are relatively difficult to

64   collect and costly to analyze, limiting their use to infer residence times of groundwater in

65   remote environments and much of the developing world. Therefore, there is great interest in

66   developing new tracers for inferring mean residence time of young groundwater (Morgenstern

67   et al., 2010; Peters et al., 2014; Tesoriero et al., 2005).
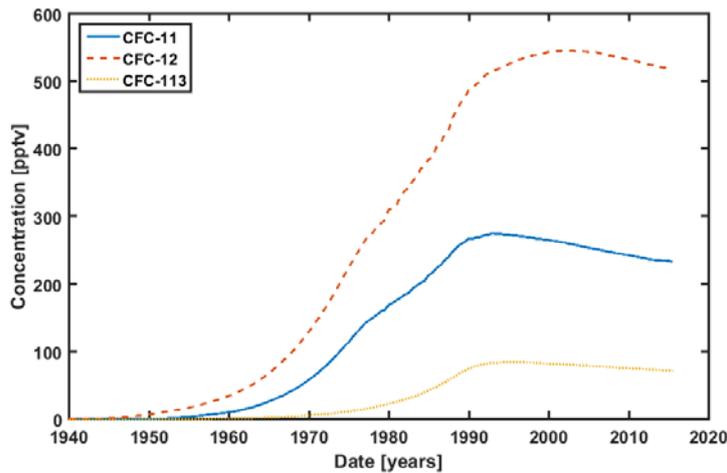
68

69   **Figure 1**: Atmospheric time series of CFC concentrations [pptv] since 1940. The lack of variations since

70   the 2000s limits their resolution in the last 20 years. Adapted from (Cook and Herczeg, 2000).

71   One promising family of potential groundwater tracers is natural weathering products

72   such as Ca^{2+}, Na^+, and dissolved silica (DSi) (Abbott et al., 2016). DSi has been found to be

73   correlated with apparent age in several site-specific studies (Bohlke and Denver, 1995; Burns

74   et al., 2003; Clune and Denver, 2012; Denver et al., 2010; Edmunds and Smedley, 2000;

75   Kenoyer and Bowser, 1992; Kim, 2002; Lindsey et al., 2003; Morgenstern et al., 2015;

76   Morgenstern et al., 2010; Peters et al., 2014; Rademacher et al., 2001; Stewart et al., 2007;

77   Tesoriero et al., 2005). However, variability of weathering rates has not been precisely

78   investigated and DSi has rarely been considered a robust tracer of groundwater age, though it

79   has been used as a relative indicator of residence time (Beyer et al., 2016; Edmunds and

80   Smedley, 2000). Two specific challenges to using DSi as a widespread proxy of mean

81   residence times are: 1. DSi lacks a time-based modeling framework and 2. it is unknown if

82   silicate weathering rates are stable enough at geologic formation to regional scales to

83   practically exploit DSi concentration.

84   In this context, we developed a new approach using groundwater DSi to determine

85   residence time distributions (RTDs) by calibrating apparent silicate weathering rates with

4

86   atmospheric groundwater age tracers (CFCs). We were motivated by the following questions:

87   1. Over what timescales can DSi be used as a tracer of groundwater age? 2. How variable is

88   the rate of silicate weathering among shallow aquifers, i.e. a few tens of meters deep, with

89   different lithology? We hypothesized that a simple zero-order kinetic reaction could simulate

90   weathering rate in shallow aquifers, because hydrolysis would remain transport-limited to

91   thermodynamically-limited on decadal timescales (detailed in section 2.1). Conversely, a

92   time-variant weathering rate (i.e. a first order kinetic reaction) would be necessary to account

93   for mineral equilibrium limitation in aquifers with longer residence times and a broader range

94   of residence times (Appelo and Postma, 1994; Maher, 2010). We tested these hypotheses by

95   modeling residence time distributions (RTDs) and weathering dynamics in 5 shallow

96   crystalline aquifers with contrasting lithology in Brittany and the Vosges Mountains, France.

97   We used conventional groundwater chemistry and dissolved CFCs from agricultural and

98   domestic wells to calibrate chemodynamic models for each catchment, using an inverse

99   Gaussian lumped parameter model to simulate RTDs. We compared our approach with

100   previous methods and explored potential applications for regional issues of groundwater

101   quality.

2   Approach, catchment description, and geochemical data

2.1   Silicate weathering and DSi concentration

104   Natural weathering products like DSi are cheap to measure and potentially contain

105   additional information on residence time distribution compared to atmospheric tracers. Indeed

106   they are sensitive to the overall residence time in both the unsaturated and saturated zones

107   (**Figure 2**), whereas atmospheric tracers are only sensitive to the residence time in the

108   saturated zone (Cook and Herczeg, 2000).
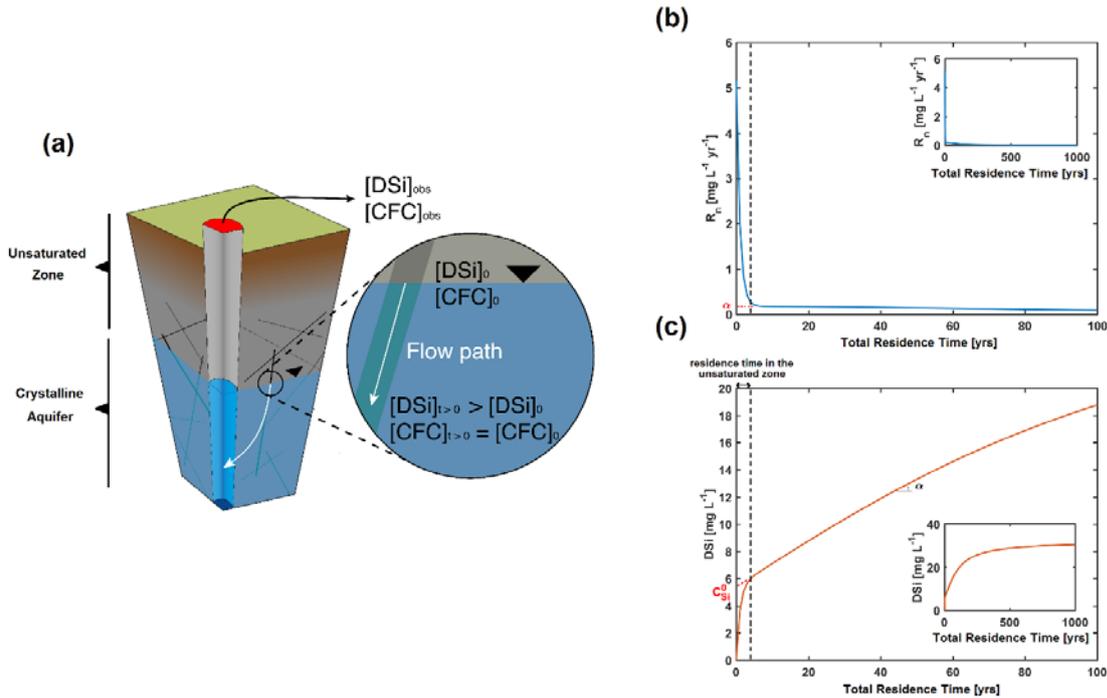
109

110 **Figure 2**: Weathering dynamics justifying our hypothesis of a zero-order kinetic reaction for the

111 weathering of silicate minerals in shallow crystalline aquifers. On the time scales considered (5-50 years),

112 the weathering rate α can be considered constant due to transport-limited and thermodynamically-limited

113 conditions (Maher, 2010). (a) Conceptual scheme illustrating the evolution of a groundwater flow path

114 from the unsaturated zone into the shallow aquifer. (b) Corresponding weathering rate evolution on two

115 different timescales. (c) Resulting DSi groundwater concentration evolution along a groundwater flow path.

116   Weathering is a rate-limited, non-equilibrium reaction consisting of physical, chemical,

117 and biological processes that occur when mineral surfaces (e.g. bedrock) are exposed to water

118 flow (Anderson et al., 2002). Weathering occurs in virtually all terrestrial environments

119 including soils, sediments, and subsurface aquifers, and depends partly on the time that

120 groundwater has spent in contact with the rock (Maher, 2011). Silicate weathering is the

121 predominant weathering process because silicate minerals constitute more than 90% of the

122 earth's crust (White, 2008).

123   As water moves through porous or fractured silicate substrate, it dissolves some silica

124 by hydrolysis (Maher, 2010). When surface water enters the subsurface, the initial rate of

125 silica hydrolysis is determined solely by the contact area between water and rock (*surface-*

126 *limited weathering*). As water percolates deeper, DSi concentration increases at the rock-

127 water interface, slowing hydrolysis unless diffusive and advective mixing remove weathering

128 products from the interface (*transport-limited weathering*). Finally, as DSi concentration in

129 the whole water mass approaches saturation, second-order equilibrium reactions control

130 hydrolysis through precipitation of secondary phases (*thermodynamically-limited weathering*)

131 (Ackerer et al., 2018; Lucas et al., 2017; Maher, 2010). Consequently, hydrologic processes

132 directly mediate weathering rate, because the speed and routing of water flow control the

133 transport of solute and the cumulative mineral surface encountered by a volume of water.

134   Differences in weathering rates along and among flow lines can create spatial variations

135 in DSi concentrations, depending on multiscale dispersive and mixing transport processes

136 (Gelhar and Axness, 1983). While the signature of detailed water-rock interactions is

137 progressively erased by mixing processes, the homogenized concentration is more

138 representative of mean weathering rate. Bulk transport models, including lumped parameter

139 models, have been developed to analyze the distribution of residence times making up a mean

140 value on the basis of realistic transport conditions (Green et al., 2014; Haggerty and Gorelick,

141 1995; Maloszewski and Zuber, 1996). Because these models simulate recharge conditions and

142 transfer processes through time, they can integrate both atmospheric and lithologic tracers,

143 providing a flexible framework for inferring transport and weathering information from

144 multiple proxies of fundamental physical and chemical processes (Abbott et al., 2016;

145 Marçais et al., 2015). Specifically, lumped parameter models overcome practical limitations

146 in inferring weathering rates and determining residence times (e.g. determining the mixing

147 that led to observed CFC concentrations), by explicitly accounting for vertical sample

148 integration in wells and the diversity of flow paths contributing to that point (Maher and

149 Druhan, 2014; Marçais et al., 2015)

150 **2.2 Catchment description**

151   We assessed the suitability of DSi as a groundwater age tracer with data from five

152 catchments. Four of the five study catchments (**Figure 3**) are located in Brittany, France,

153 where the climate is oceanic and average precipitation ranges from 900 mm yr^{-1} in Plœmeur

154 and Guidel catchments to 960 mm yr^{-1} in Pleine Fougères and Saint Brice catchments

155 (Jiménez-Martínez et al., 2013; Thomas et al., 2016a; Touchard, 1999). Land use in all these

156 catchments is dominated by agriculture (i.e. 70-90% of arable land used for row crops) and in

157 one of them, the aquifer is intensively pumped for municipal water supply (Plœmeur,

158 hereafter the *pumped catchment*; pumping rate = 110 m^3 hr^{-1}). The Pleine Fougères, Saint

159 Brice and Guidel catchments are designated hereafter as *agricultural catchments* 1, 2, and 3,

160 respectively. The fifth catchment is located in the Vosges Mountain (Strengbach, hereafter the

161 *mountainous catchment*), in a forested region with elevation ranging from 880 to 1150 m, an

162 oceanic mountainous climate, and average annual precipitation of 1400 mm yr^{-1} (Pierret et al.,

163 2014; Viville et al., 2012). Though all 5 catchments are underlain by crystalline bedrock

164 (**Figure 3**), they differ in underlying lithology (granite or schist) and catchment size (from 0.8

165 to 35 km^2; **Table 1**). They all have slightly acidic groundwater with pH between 5 and 7

166 (**Table 1**). Groundwater temperature is more variable among the catchments, ranging from

167 8°C in the high-elevation mountainous catchment to ~13°C in the lowland Brittany

168 catchments. The pumped catchment displays the strongest spatial variability of groundwater

169 temperature, varying between 12 and 17°C due to the pumping activity (**Table 1**). Detailed

170 site information is provided in the supplementary information and the references are listed in

171 **Table 1**.
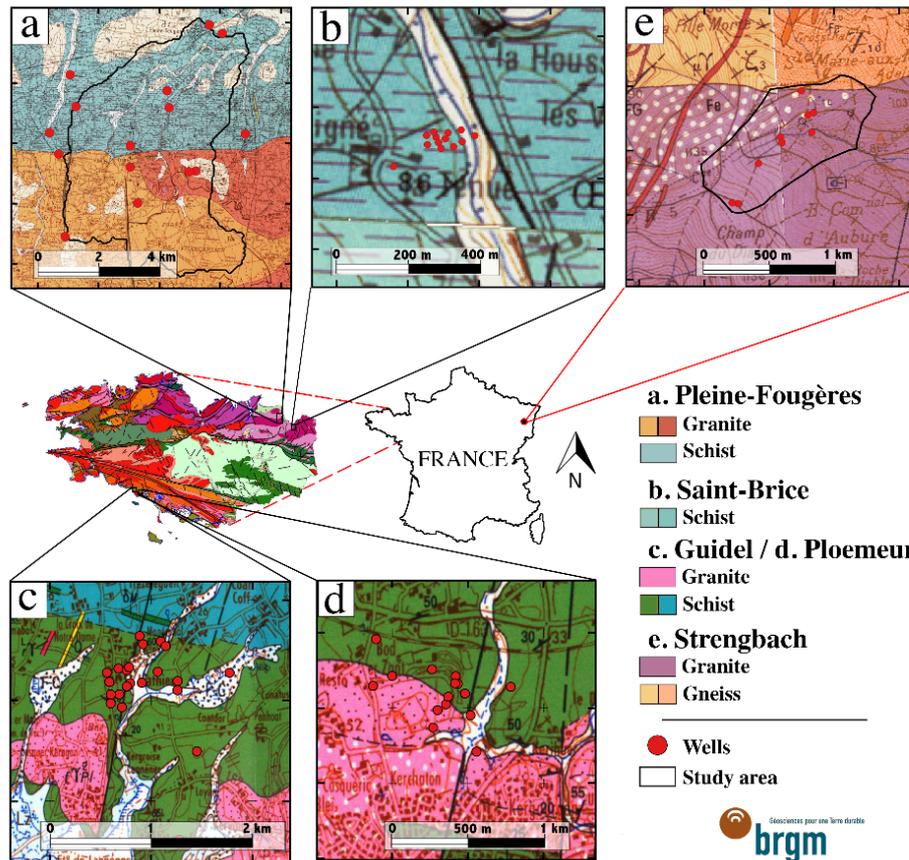
Figure 3: Site locations on the geological map of Brittany (center-left) with detailed site maps of lithology and well location for (a) Pleine Fougères, (b) Saint Brice (c) Guidel, and (e) Plœmeur, which is a pumping site for drinking water supply. (d) Strengbach is a headwater located in the Vosges Mountains (east part of France). Adapted from the Bureau de Recherches Géologiques et Minières (BRGM) data.

2.3   Geochemical data

For each catchment, we analyzed CFC-12, CFC-11, CFC-113, and DSi concentrations determined during field campaigns between 2001 and 2015. We only used sampling dates where DSi and at least one CFC were simultaneously measured. Because the sampling of DSi and CFCs is relatively straightforward (a filtered and acidified water sample for DSi and water collected in a stainless-steel vial for CFCs), there were multiple, spatially-distributed replicates for each catchment corresponding to different sampling wells or sampling campaigns (i.e. 32 replicates on average for each catchment, see **Table 1**). DSi was quantified

185   as H_4SiO_4 (mg L^{-1}), from 0.2µm filtered and acidified samples by inductively coupled plasma

186   mass spectrometry (ICP-MS) at the Geoscience Rennes laboratory, with an uncertainty of

187   ±2% (Bouhnik-Le Coz et al., 2001; Roques et al., 2014b). CFC concentrations were measured

188   by purge and trap gas chromatography at the CONDATE EAU laboratory, at the OSUR in the

189   University of Rennes 1 (France), with a precision of ±4% for high concentrations and ±20%

190   for samples near the quantification limit (0.1 pmol L^{-1}; Labasque et al. (2014); Labasque et al.

191   (2006)). Dissolved concentrations were converted to atmospheric partial pressures (pptv) with

192   Henry's law, considering gas solubility and excess air effects (Busenberg and Plummer,

193   1992). Samples showing obvious contamination with CFCs were excluded from the analysis

194   (7% of samples were above the maximum atmospheric concentration of CFC).

195   Contamination, which occurred primarily at the pumped catchment, was likely due to

196   manufacturing or maintenance activities in the nearby military airport.

Catchment ID	Catchment Name	Area (km²)	Lithology	Number of Wells	Number of data (number of data used)	Percentage of polluted data	pH	Water Temperature (°C)	Unsaturated Zone Thickness (m)	Supplementary Information	References
Agricultural catchment 1	Pleine Fougères	35	Granite (50%) and Schist (50%)	18	21(20)	0%	5.2-7.2	11-14	-	Moderate agricultural inputs	(Kolbe et al., 2016)
Agricultural catchment 2	Saint Brice	1	Mainly Schist	11	48(45)	6%	5.3-7.1	12-14.6	2.2-5.1-9.4	Moderate agricultural inputs	(Roques et al., 2014b)
Agricultural catchment 3	Guidel	2.9	Schist	10	18(18)	0%	-	14-14.7	0.5-5.3-18	1 km from the sea - Moderate agricultural inputs	(Bochet, 2017; Bochet et al., under revision)
Pumped catchment	Plœmeur	2.5	Granite and Schist	16	65(58)	11%	5.4-6.5	12-17.3	7-12-30	Pumping site	(Le Borgne et al., 2006; Leray et al., 2012)
Mountainous catchment	Strengbach	0.8	Granite	11	17(17)	0%	5.6-7	7.6-9.3	0-2.5-6	Mountainous headwater (Vosges)	(Chabaux et al., 2017; Viville et al., 2012)

197 **Table 1**: Characteristics of the study sites. The sites display contrast in size, lithology, and geochemical conditions especially regarding water temperature. For the

198 unsaturated zone thickness, the minimum, average and maximum thickness of the unsaturated zone (m) are reported.

3 Modelling residence times and silicate weathering rates

To test our regional uniformity hypothesis, we simultaneously inferred residence times and silicate weathering rates for all five catchments, using data from the spatially distributed replicates within each catchment to derive representative weathering rates. We developed a standardized methodology requiring minimal a priori information to calibrate the lumped parameter models for the determination of RTDs. CFCs and DSi concentrations were jointly used to calibrate the lumped parameter models for each replicate (i.e. well), while weathering rates were optimized for each catchment to minimize the overall mismatch between modeled and measured concentrations. Following this procedure, silicate weathering rates were derived from DSi concentrations calibrated with CFC concentrations, which showed broad variability in mean residence time among sites.

Because CFC concentrations depend primarily on the date of groundwater recharge, while DSi concentration depends on water-rock interactions, these two tracers potentially contain complementary information about RTDs. In the following sections, we present the assumptions about weathering and types of RTDs, and then detail the calibration strategy aiming at determining weathering at the scale of the catchment and RTD properties for each well.

3.1 Weathering assumptions

Chemical weathering of silicate minerals is the net result of the dissolution of primary silicate minerals minus the precipitation of secondary mineral formation (Anderson and Anderson, 2010). To model the effect of residence times on overall observed DSi concentrations, we considered that precipitation and dissolution rate constants lead to a net weathering rate α [mg L^{-1} yr^{-1}], which corresponds to the enrichment rate of groundwater in DSi.

223   At the intermediate scale (10s to 100s of meters), this net weathering rate encounters a

224   rapid transition from surface-limited to transport-limited weathering. During this transition,

225   weathering rates may differ in the unsaturated zone as minerals differ from the deeper

226   unaltered zone and water contains lower DSi concentrations, which together favor surface

227   reaction-limited processes. While we did not estimate unsaturated zones weathering rates, we

228   did account for differences in DSi concentration at the water table (see next paragraph). Time-

229   based observations in crystalline formations show that weathering rates do not depend on

230   residence times for groundwater older than few months to decades, due to transport and

231   thermodynamic controls, which sustain the weathering (Ackerer et al., 2018; Maher, 2010;

232   White and Brantley, 2003). Given that the shallow crystalline aquifers investigated in this

233   study have CFC apparent ages greater than 25 years (Ayraud, 2005; Ayraud et al., 2008;

234   Kolbe et al., 2016; Leray et al., 2012; Roques et al., 2014a), we assumed that α stays

235   constant i.e. that the net weathering follows a zero-order kinetic reaction.

236   The DSi concentration from the dissolution of silicates in the unsaturated zone is

237   assumed to lead to an initial DSi concentration C_{Si}^0, which does not depend on the

238   groundwater residence time t (i.e. the amount of time water spends in the unsaturated zone

239   may be unrelated to the subsequent residence time in the aquifer). t only represents the

240   residence time in the aquifer because it is inferred from CFC concentrations, which

241   equilibrate at the water table (**Figure 2**a). Therefore, assuming a constant weathering rate α

242   and an initial DSi concentration C_{Si}^0 reached at the water table results in a linear expression of

243   the DSi concentration as a function of the residence time t [yr]:

$$C_{Si}^{prod}(t) = \begin{cases} \alpha\, t + C_{Si}^0 & \text{if} \quad t < t_{max}, \\ C_{Si}^{max} = \alpha\, t_{max} + C_{Si}^0 & \text{if} \quad t \ge t_{max}, \end{cases} \tag{1}$$

244 where t_{max} is the time at which groundwater becomes saturated in DSi (i.e. precipitation or

245 removal equals dissolution). Indeed, at larger scale, mineral equilibrium can be reached.

246 However, recent hydrogeochemical modeling of weathering in the mountainous catchment

247 showed that silica equilibrium is not reached until kilometers of transport, much farther than

248 typical flow distance between recharge areas and sampling wells or surface water features

249 (Ackerer et al., 2018; Kolbe et al., 2016; Lucas et al., 2017). Additionally, for many

250 catchments there is a negligible contribution of groundwater with residence times longer than

251 100 years (age at which the groundwater is likely to encounter DSi saturation) as shown by

252 the presence of CFCs in the groundwater of these catchments. Therefore, C_{Si}^{prod} only depends

253 on residence time t, weathering rate α and initial DSi concentration C_{Si}^0 at the water table.

254 **3.2 Modeling groundwater mixing**

255 Multiple geological, topographical, and hydraulic factors influence RTDs. Distributed

256 groundwater flow and transport models were previously developed for the agricultural

257 catchment 1 and the pumped catchment, showing that the general shape of the RTDs can be

258 well approximated by an inverse Gaussian function in most cases (Kolbe et al., 2016; Marçais

259 et al., 2015). Inverse Gaussian distributions have proved especially efficient for providing

260 accurate predictions of distribution quantiles and integrated renewal times within the time

261 range where information can theoretically be extracted from CFC tracers (i.e. 0-70 years,

262 **Figure 1**). Previous studied sites have also shown that the choice of the lumped parameter

263 model is not critical as long as it has two parameters and is unimodal (Eberts et al., 2012;

264 Kolbe et al., 2016; Marçais et al., 2015). Inverse Gaussian distributions have the additional

14

265 advantage of being physically grounded as they are the solution of the 1D advection

266 dispersion equation:

$$f_{\mu,\sigma}(t) = \frac{1}{\sigma}\sqrt{\frac{\mu^3}{2\pi t^3}}\exp(-\frac{\mu(t-\mu)^2}{2\sigma^2 t}),\qquad\qquad (2)$$

267 where t is the residence time, μ is mean time and σ is the standard deviation. The two

268 degrees of freedom of an inverse Gaussian distribution are sufficient to adapt to most

269 observed hydraulic conditions found in upland sites, which show narrow distributions similar

270 to Dirac distributions, and in lowland sites near the surface flow outlet, which express more

271 exponential shapes (Haitjema, 1995). We therefore used inverse Gaussian distributions for all

272 catchments, though a different lumped parameter model's choice could be easily implemented

273 if hydraulic conditions required it (Leray et al., 2016).

274   Inferring RTDs with an inverse Gaussian LPM requires determining two parameters:

275 the mean residence time μ and the standard deviation σ of the distribution. For a given

276 Inverse Gaussian RTD $f_{(\mu,\sigma)}$, the concentrations in CFCs can be modeled as:

$$
\begin{aligned}
C_{CFC-12}^{\text{mod}}(t_s,\mu,\sigma) &= \int_{0}^{+\infty}\mathcal{C}_{CFC-12}(t_s-u)\cdot f_{(\mu,\sigma)}(u)\,du\\
C_{CFC-11}^{\text{mod}}(t_s,\mu,\sigma) &= \int_{0}^{+\infty}\mathcal{C}_{CFC-11}(t_s-u)\cdot f_{(\mu,\sigma)}(u)\,du\quad,\\
C_{CFC-113}^{\text{mod}}(t_s,\mu,\sigma) &= \int_{0}^{+\infty}\mathcal{C}_{CFC-113}(t_s-u)\cdot f_{(\mu,\sigma)}(u)\,du
\end{aligned}
\qquad (3)
$$

277 where u is the residence time, t_s is the sampling date, $t_s - u$ is the recharge date (when the

278 water reaches the water table) and $\mathcal{C}_{CFC}$ is the corresponding CFC atmospheric time series

279 (**Figure 1**). Integrating over all the potential residence times, the product of the RTD $f_{(\mu,\sigma)}$

280 with the CFC concentration present at the water table at $t_s - u$ gives the modeled CFC

281 concentration. Similarly, the modeled concentration in DSi can be expressed as:

$$C_{Si}^{\mathrm{mod}}(\alpha, C_{Si}^0, \mu, \sigma) = \int\limits_0^{+\infty} C_{Si}^{prod}(\alpha, C_{Si}^0, u) \cdot f_{(\mu,\sigma)}(u)\, du, \tag{4}$$

282 where C_{Si}^{prod} is the DSi concentration produced during the residence time u via weathering

283 (equation (1)). Equations (3) and (4) give the modeled concentrations of CFCs and DSi,

284 which depend on the LPM parameters (μ, σ), and on the catchment-based weathering

285 parameters (α, C_{Si}^0), related to site characteristics.

3.3 Calibration strategy: inferring conjointly RTDs and silicate weathering rates

287 With N wells on a given catchment and N concentrations of CFCs and DSi

288 $(C_{CFC-12_k}^{mes}, C_{CFC-11_k}^{mes}, C_{CFC-113_k}^{mes}, C_{Si_k}^{mes})_{1 \le k \le N}$, the calibration strategy consisted in optimizing

289 together (i.e. for the N datasets) the weathering rate α, the initial concentration of DSi C_{Si}^0,

290 and the best inverse Gaussian LPMs $(\mu_k, \sigma_k)_{1 \le k \le N}$ for each of the N wells. We defined the

291 following objective function to optimize the calibration:

$$\Phi(\alpha, C_{Si}^0, \mu_1, \sigma_1, \ldots, \mu_N, \sigma_N) =$$

$$\frac{1}{3N}\sum_{k=1}^{N}\left[\left| \tilde{C}_{Si\ k}^{mes} - \tilde{C}_{Si\ k}^{mod}(\alpha, C_{Si}^0, \mu_k, \sigma_k) \right| + \right. $$

$$(5)$$

$$\min\quad \tilde{C}_{CFC-12k}^{mes} - \tilde{C}_{CFC-12k}^{mod}(t_{s_k}, \mu_k, \sigma_k) + \tilde{C}_{CFC-11k}^{mes} - \tilde{C}_{CFC-11k}^{mod}(t_{s_k}, \mu_k, \sigma_k),$$

$$\tilde{C}_{CFC-12k}^{mes} - \tilde{C}_{CFC-12k}^{mod}(t_{s_k}, \mu_k, \sigma_k) + \tilde{C}_{CFC-113k}^{mes} - \tilde{C}_{CFC-113k}^{mod}(t_{s_k}, \mu_k, \sigma_k),$$

$$\tilde{C}_{CFC-11k}^{mes} - \tilde{C}_{CFC-11k}^{mod}(t_{s_k}, \mu_k, \sigma_k) + \tilde{C}_{CFC-113k}^{mes} - \tilde{C}_{CFC-113k}^{mod}(t_{s_k}, \mu_k, \sigma_k)\quad ,$$

292   where $\tilde{C}$ are the standardized and centered values of C. In equation (5), the minimum

293   conveys that we only retain the two most coherent CFC concentrations with their respective

294   modeled counterparts out of the three CFC concentrations available (Jurgens et al., 2012).

295   Because of some non-convexity of the objective function Φ, we use a two-step

296   optimization method with an initial calibration of (α, C_{Si}^0) with the simulated annealing

297   Monte-Carlo method in MATLAB (Ingber, 2000), and a second gradient-based Levenberg-

298   Marquardt optimization to complete the reduction of the set of parameters. Using this

299   methodology, weathering rates were compared among the catchments to test for regional

300   differences in weathering rate.

301   **4   Results**

302   We first report observed CFC and DSi concentrations for the different catchments and

303   then use the methodology presented in section 3 to derive the catchment-level weathering

304   rates and individual well RTDs.

4.1 Observed CFC and DSi concentrations

The relationship between CFCs and DSi was generally negative, though the strength of the relationship and range of values varied by catchment (see **Figure 4**). Given the theoretical relationship between CFCs and DSi, **Figure 5** shows the concentrations of CFC-12 and DSi that can be reached with Inverse Gaussian RTDs, whatever their mean and standard deviations in the range of 0-100 years for the two silicate weathering rates, i.e. $(\alpha = 0.25 \, \text{mg L}^{-1}\text{yr}^{-1}, C_{Si}^{0} = 4 \, \text{mg L}^{-1})$ and $(\alpha = 0.5 \, \text{mg L}^{-1}\text{yr}^{-1}, C_{Si}^{0} = 8 \, \text{mg L}^{-1})$. Each point represents an Inverse Gaussian RTD with specific parameters. Sampling well data of the agricultural catchment 1 are shown as green triangles on the same plot for illustrative purposes and the best RTD associated for each well sampled is represented among the different Inverse Gaussian RTD by orange circles. The lower weathering scenario $(\alpha = 0.25 \, \text{mg L}^{-1}\text{yr}^{-1}, C_{Si}^{0} = 4 \, \text{mg L}^{-1})$ explained much of the variability observed in the CFC-12 and DSi concentrations, suggesting that it is closer to the *in situ* rate. The difference between the two envelopes underlines the high sensitivity of the weathering model and gives some preliminary illustration of the capacity of extracting meaningful weathering properties.

320
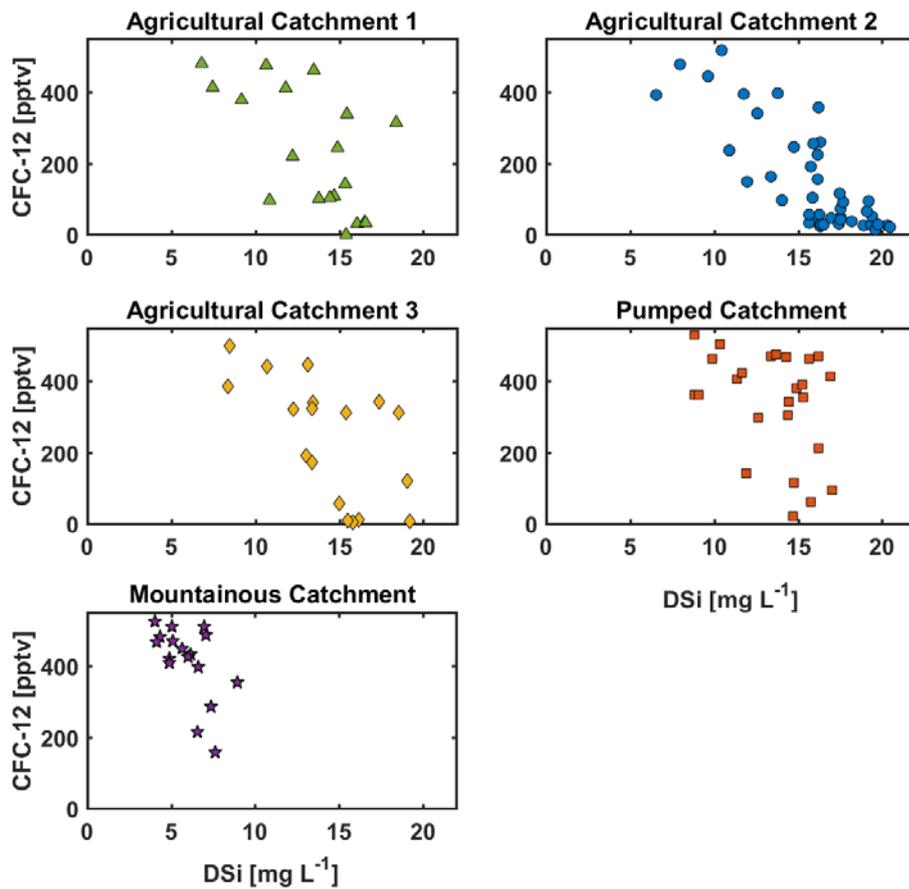
Figure 4: CFC-12 vs DSi concentrations obtained for each of the field sites.

4.2 Catchment-based optimal weathering rates

We applied the same optimization method for each of the 5 catchments. ρ (the average model error) varied significantly among catchments, with relatively small values (below 0.25) for most of the catchments, but higher values for the pumped catchment ($\rho = 1.64$; **Table 2**). Optimal weathering rates were relatively similar among catchments, especially for the agricultural catchments, which ranged from 0.20 to 0.23 mg $L^{-1}yr^{-1}$ (CV = 7%), demonstrating regional consistency among different rock types. The weathering rate was significantly slower (0.12 mg L yr^{-1}) in the mountainous catchment and significantly faster in the pumped catchment (0.31 mg L yr^{-1}).

331
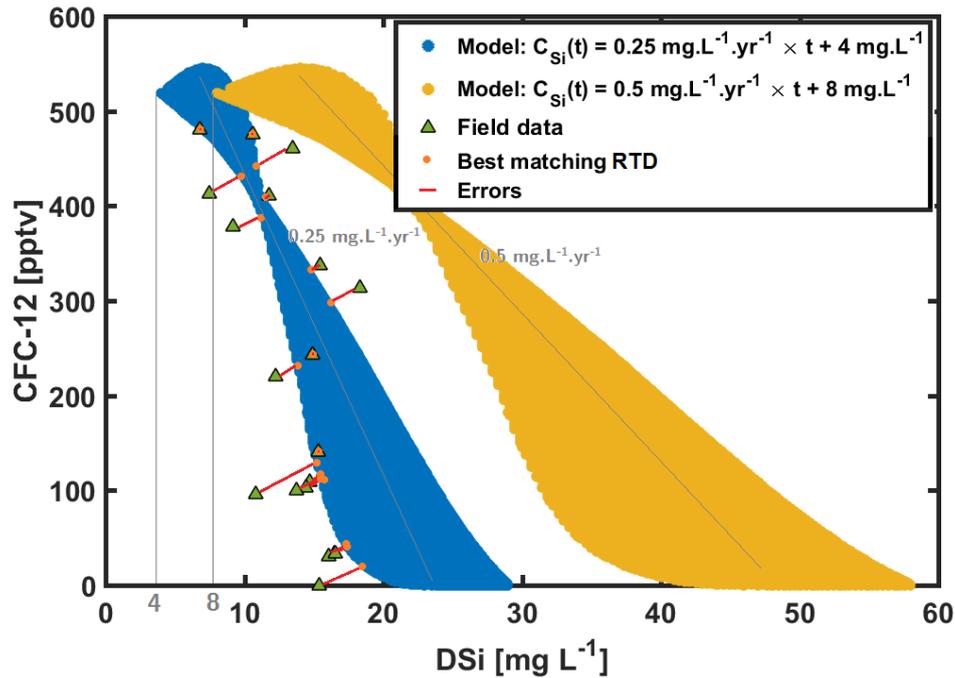
Figure 5: Calibration methodology. For each dataset representative of one site (Field data), the equation of weathering (1) is optimized by minimizing the sum of the square errors between the well data and their best matching Inverse Gaussian RTD in the RTD model ensemble. Two models ensemble are represented: the blue one with $(\alpha, C_{Si}^0) = $ (0.25 mg L^{-1} yr^{-1}, 4 mg L^{-1}) and the yellow one with $(\alpha, C_{Si}^0) = $ (0.5 mg L^{-1} yr^{-1}, 8 mg L^{-1}). Notice how C_{Si}^0 controls the horizontal position of the RTDs models in the (CFC, DSi) plot, especially for the young fraction of the RTDs (high CFC-12, low DSi) while α controls the overall DSi spreading of the models ensemble, especially for the old fraction of the RTDs (low CFC-12, high DSi).

Optimal initial DSi concentrations (C_{Si}^0) displayed some variability with a coefficient of variation of 19% among catchments. On the extremes, the mountainous catchment showed an initial DSi of 2.9 mg L^{-1} while the pumped catchment had an initial concentration of 5.0 mg L^{-1}, likely due to differences in weathering in the unsaturated zone.

Catchment	ρ [-]	α [mg L^{-1} yr^{-1}]	C_{Si}^0 [mg L^{-1}]	mean (μ) [yr]	mean (σ) [yr]
Agricultural catchment 1	*0.12*	*0.20*	*4.0*	*52*	*39*

Agricultural catchment 2	*0.26*	*0.22*	*3.8*	*60*	*32*
Agricultural catchment 3	*0.23*	*0.23*	*4.3*	*52*	*49*
Pumped catchment	*1.64*	*0.31*	*5.0*	*40*	*53*
Mountainous catchment	*0.19*	*0.12*	*2.9*	*30*	*59*

343   **Table 2**: Results obtained from the calibration. ρ is the residual (see equation (1)). α is the weathering

344   rate in mg L^{-1} yr^{-1}, C_{Si}^0, the initial DSi concentration in mg L^{-1}. The two last columns present some

345   statistics about the parameters of the inverse Gaussian distributions optimized for each well: the average of

346   the mean residence time μ in years and the average of the standard deviation σ in years of the residence

347   time distributions for each catchment.

348   **4.3   Models of RTDs**

349   The largest differences between well-level RTDs occurred in the agricultural catchment

350   2 (**Figure 6**). The wells intersecting deep productive fractures had high DSi concentration and

351   low CFC concentrations (**Figure 4**) and displayed broad RTDs between 40 and 100 years

352   (**Table 2** and yellow and purple curves in **Figure 6**). The low CFC concentrations

353   corresponded with the modeled RTDs, which indicated limited modern water (less than 15 to

354   20 years' old). High DSi concentration requires much longer timescales and can be modeled

355   as well by the contribution of residence times above 40 years. The water residence time

356   distributions of the shallow wells (blue and red curves of **Figure 6**) showed significantly

357   younger water due to the lack of the old water contributions coming from deeper fractures

358   (**Figure 6**).
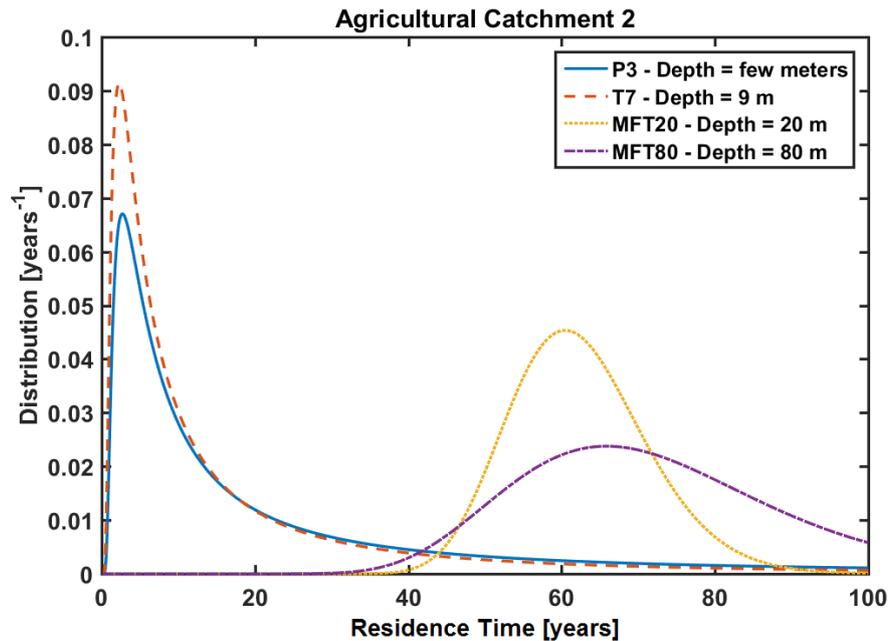
360 **Figure 6**: Illustration of the calibrated Inverse Gaussian RTD obtained on the agricultural catchment 2

361 (Saint Brice). The wells lying in the shallowest part of the aquifers have small residence times and

362 exponential shapes. The wells lying in the deepest part of the aquifer display some skewed distributions.

363   To get an idea of the type of RTDs obtained for the other catchments, we also compared

364 some statistics of the RTDs between sites, obtained with the optimization reported in **Table 2**.

365 All catchments have RTDs with mean residence times, which range on average between 30

366 years for the mountainous catchment and 60 years for the agricultural catchment 2.

367 **4.4   Relations between DSi and mean residence times**

368   A byproduct of the calibration of the inverse Gaussian lumped parameter model for the

369 DSi and CFC concentrations was the relation between the modeled mean residence times and

370 the observed DSi concentrations here shown for the three agricultural catchments located in

371 Brittany (**Figure 7**). For each catchment, the relation appeared to be linear, reinforcing the

372 consistency between the observed and modeled concentrations, and providing support for the

373 assumptions of the modeling approach. More specifically, the direct proportionality of the

374 DSi concentration to the mean residence time validated weathering assumptions modeled by a

375   zero-order kinetic reaction (equation (1)). The linear relations were also similar among

376   catchments with coefficients of variation of respectively 7% and 6%, for the different

377   weathering rates and the initial DSi concentration of the agricultural catchments.
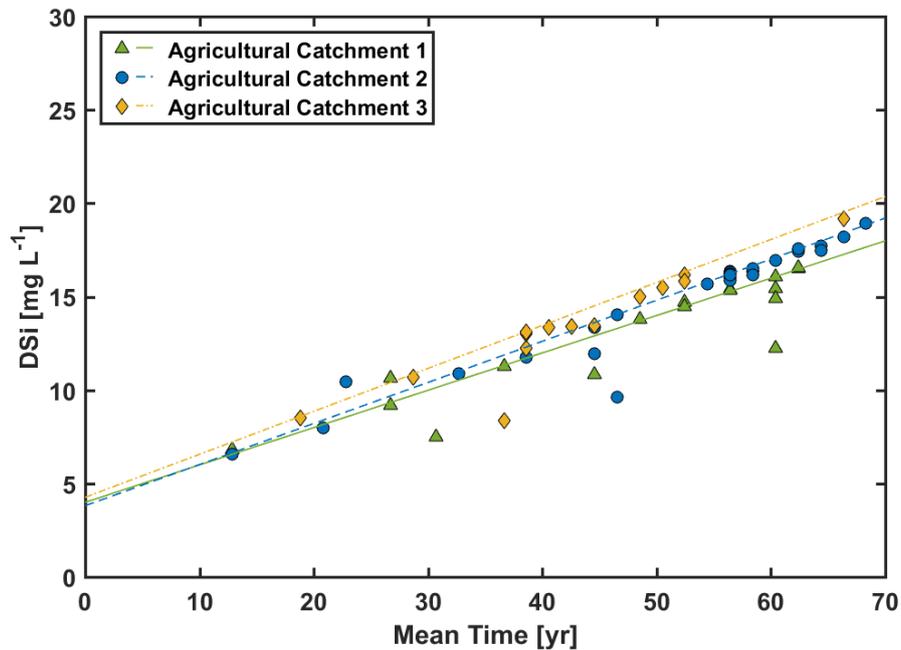
378

379   **Figure 7**: Measured DSi concentration versus the optimized mean residence time of the inverse Gaussian

380   lumped distribution for three of the Brittany sites. Straight lines represent the optimized weathering law for

381   each of the sites. Note that it fits the measurements. Considering a constant weathering rate allows direct

382   interpretation of DSi apparent ages into mean residence times.

383   We compared these modeled mean residence times obtained with the CFC and DSi

384   concentrations with the mean residence times calibrated only with the CFC concentrations

385   (**Figure 8**). These CFC-only mean residence times were obtained using equation (1) without

386   considering DSi concentrations. For each of the wells in the different catchments, the mean

387   residence times obtained were quite consistent, especially for mean residence times ranging

388   between 0 and 50 years. For such a time range, a linear regression gives $\mu_{DSi-CFCs} =$

389    $1.03 \, \mu_{CFCs}$ with a R^2 of 0.36.
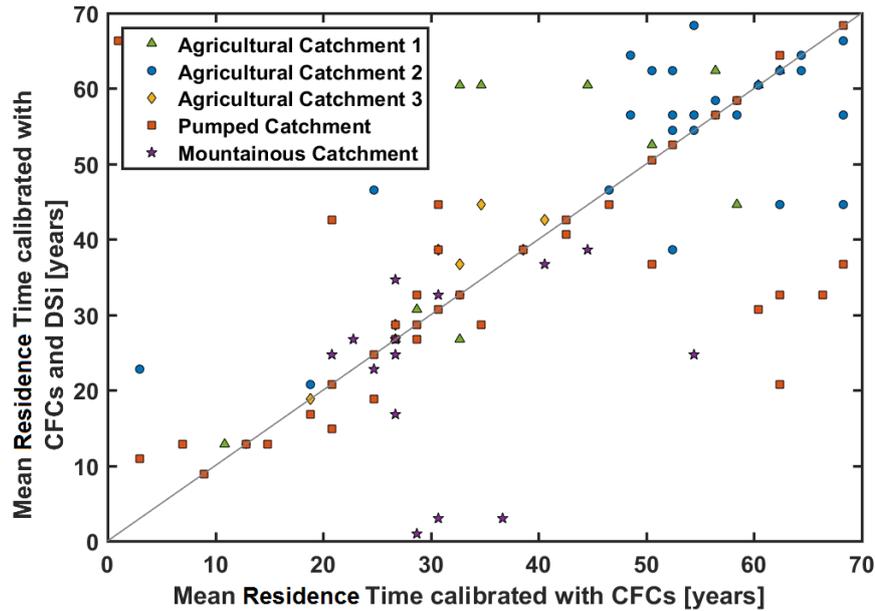
Figure 8: Comparison between the mean residence time obtained with CFCs and DSi concentrations with those obtained only with the CFC concentrations.

5   Discussion

While DSi has been used as a site-specific indicator of groundwater residence time (Burns et al., 2003; Kenoyer and Bowser, 1992; Morgenstern et al., 2010; Peters et al., 2014), it was unknown how consistent silica weathering rates were, and consequently if DSi could be a useful tracer at regional scales. In this study, we evaluated the use of DSi for groundwater dating at four catchments in Brittany and one catchment in the Vosges Mountains. The data and our simulations supported the hypothesis that silica weathering can be described by a zero-order kinetic reaction at the catchment scale, and we calibrated silicate weathering laws using CFC atmospheric tracers. We found that DSi provided complementary information to CFC atmospheric tracers on RTDs. The relative stability of weathering rates among the Brittany agricultural catchments validates the use of DSi as a regional groundwater age proxy. We discuss below how these weathering rates may be modified by climatic context (from the oceanic conditions of Brittany to the mountainous climate of the Vosges) and by external

406   factors, e.g. groundwater abstraction. Finally, we discuss the use of DSi for evaluating

407   residence times in unsaturated zones and compare these optimized silicate weathering rates to

408   weathering rates estimated in previous studies.

5.1   Practical use of DSi as a proxy of groundwater residence time

410   DSi concentration appears to be a highly complementary tracer to atmospheric tracers

411   such as CFCs. For example, at the agricultural catchment 2 (**Figure 6**), the comparison of

412   wells of different depths (shallow wells for P3 and T7, and deeper wells for MFT 20 and

413   MFT80) revealed that DSi concentration can infer the RTD even when CFCs are not

414   discriminating because they are below their detection limit for older ages (> 70 years) or

415   during the flat portion of their atmospheric trend (i.e. the last 0-20 years). These time ranges

416   where CFCs are less informative are further exacerbated by the widening of the concentration

417   area reachable by the inverse Gaussian function towards lower and higher CFC-12

418   concentration (**Figure 5**). For such CFC range (for example, for CFC-12 between 450 and

419   550 pptv and between 0 and 50 pptv), DSi is particularly useful to better characterize RTD.

420   The comparison between the modeled mean residence times and those calibrated only with

421   CFCs (**Figure 8**) also displayed an increased consistency for the time range between 0 and 50

422   years. For mean residence times above 50 years, DSi appears to give complementary

423   information to mean residence times from CFCs as depicted by the increased variability of

424   mean residence times around the identity line $y = x$.

425   The bulk linear relation for weathering rate (equation (1)) is also of interest for dating

426   purposes as DSi concentrations can be seen as a direct proxy of the mean residence time

427   (**Figure 7**), which is not the case for other tracers such as CFCs (**Figure 1**) (Leray et al., 2012;

428   Marçais et al., 2015; Suckow, 2014). While this result has been obtained with a specific

429   Lumped Parameter Model (inverse Gaussian), it is generally applicable for a broad range of

430   distributions as it relies on the zero-order weathering assumption that leads to a linear

431   dependence of the DSi concentration on residence times (equation (1)).

432   Even if the small residuals obtained in **Table 2** indicate that the inverse Gaussian model

433   may be appropriate for RTDs, other types of distributions, like the Gamma distribution, can

434   be tested to assess the sensitivity of the LPM choice to the RTD-related prediction. For the

435   agricultural catchment 1 and the pumped catchment, shapes of the Inverse Gaussian LPM as

436   well as the statistics obtained regarding the optimized RTDs (**Table 2**) are consistent with

437   results obtained synthetically from calibrated 3D flow and transport models developed for

438   these aquifers (Kolbe et al., 2016; Leray et al., 2012).

439   The 5 to 100 years' time range of the RTDs observed here is the most favorable case for

440   using DSi for groundwater dating since it leads to thermodynamic-limitation conditions which

441   sustains chemical weathering (Maher, 2010). Even though weathering rates α might be quite

442   variable between different crystalline rock types, the fluid-rock contact time controls the

443   evolution of DSi concentrations for residence times ranging from years to decades (5-100

444   years) where dissolution is the dominant process. On the contrary, attainment of the mineral

445   equilibrium restricts the use of DSi for estimating longer residence times (>300 years) when

446   dissolution is balanced by re-precipitation (Edmunds and Smedley, 2000).

447   **5.2   Stability of silica weathering rates at the regional scale**

448   *5.2.1   DSi as a robust regional groundwater age proxy*

449   Our results indicate that DSi can be used as groundwater age tracing tool in relatively

450   diverse geologic contexts, as indicated by the consistency of the weathering rates for the

451   different Brittany catchments (**Figure 7**). This homogeneity suggests that only a few mineral

452   phases are responsible for silica production in the studied residence-time range; typically

453   phyllosilicates, plagioclase, and accessory minerals such as apatite are the major sources of

454   silica (Aubert et al., 2001). Applying a uniform weathering rate (0.22 mg L^{-1} yr^{-1}) and initial

455   DSi concentration (4.0 mg L^{-1}) can provide a first order estimate of mean residence time, as

456   displayed by the blue curve presented in **Figure 9** compared to the weathering rates of each of

457   the Brittany catchments displayed in **Figure 7**. The relatively small error associated with

458   catchment specific differences justifies the possible use of DSi as a regional groundwater

459   dating tracer, as long as a weathering law can be applied based on similar catchments or land

460   lithologies. If more complete modeling is available, the choice between weathering laws can

461   be bypassed by directly solving the mass balance of the geochemical water content (Burns et

462   al., 2003).
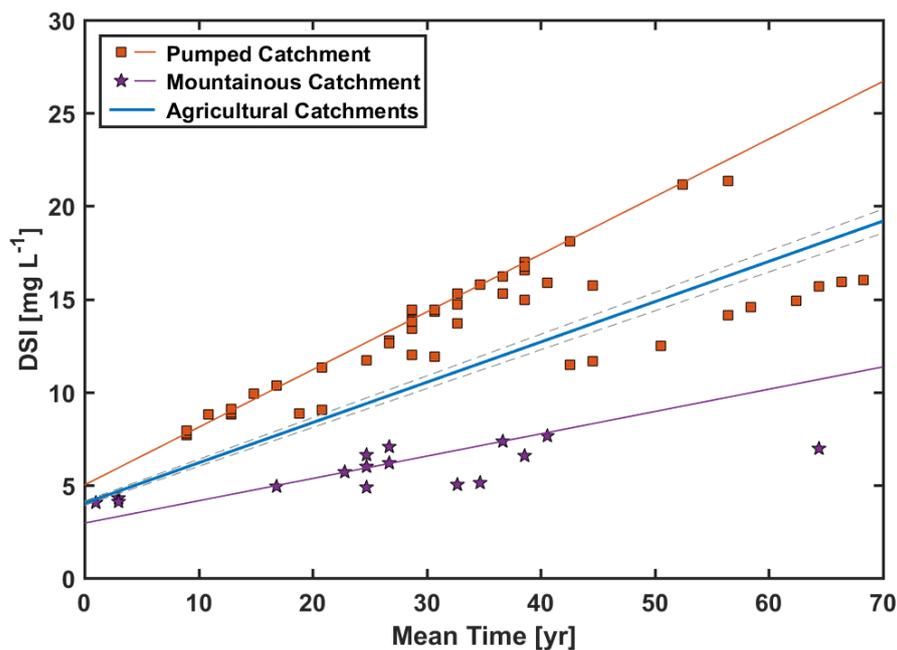
463

464   **Figure 9**: DSi concentrations versus the optimized mean residence time of the inverse Gaussian displayed

465   for each wells for the mountainous and the pumped catchment. Straight lines represent the optimized

466   weathering law for each of the sites. Note that it fits the measurements. Considering a constant weathering

467   rate enables to indistinctly consider Si apparent ages and mean residence times.

468   Silicates are ubiquitous in most geological matrices, including crystalline and

469   sedimentary rocks (Iler, 1979). There is some evidence for using DSi as a groundwater age

470   proxy in other rock types (e.g. sedimentary rocks coming from glacial deposits, see section

471   5.4) (Becker, 2013; Kenoyer and Bowser, 1992). DSi concentration is widely measured and

472   accessible through public observatories and databases (Abbott et al., 2018; De Dreuzy et al.,

473   2006; Thomas et al., 2016b). While previous studies have shown dependency of weathering

474   rates on lithology and climate (White and Blum, 1995; White et al., 1999; White et al., 2001),

475   DSi might be considered a "contextual tracer", allowing at least local and potentially regional

476   groundwater dating (Beyer et al., 2016).

477   A major advantage of DSi is that it persists in open surface waters (e.g. lakes and

478   streams), whereas other tracers of intermediate transit times such as ^{3}H/He and CFCs quickly

479   equilibrate with the atmosphere. Additionally, because artificial sources are few and

480   background concentration is usually high, DSi is robust to contamination, unlike CFCs, which

481   cannot be in contact with the atmosphere during sampling nor with any plastic surfaces

482   (Labasque et al., 2014). However, uptake of DSi by some vegetation and diatoms could

483   potentially limit the use of DSi in some environments especially during the growing season

484   (beginning of summer) (Delvaux et al., 2013; Pfister et al., 2017). This uptake is more likely

485   in large rivers systems where DSi spend enough time to be effectively captured by diatoms

486   whereas it is less prone to occur in headwaters systems with much smaller stream residence

487   times (Hughes et al., 2013). To track this potential additional process into account, diatom

488   uptake could be modeled (Thamatrakoln and Hildebrand, 2008) and/or isotopic DSi ratios

489   could be investigated to link in stream DSi concentration to mean transit time (Delvaux et al.,

490   2013).

491   *5.2.2   Comparison between the agricultural catchments and the mountainous catchment*

492   Weathering rates were relatively constant within a given regional geological and climatic

493   context (e.g. for the three catchments in Brittany), but they were significantly different from

494   the mountainous catchment (Vosges Mountains). Differences in lithology could control

495   overall weathering rates, but this was not supported by the observed homogeneity of the

496   weathering rate across different lithologies (section 5.2.1). Acidity could not either explain

497   this variability, as pH was comparable for all the catchments (**Table 1**). The lower rates in the

498   mountainous catchment may be due to a difference in climatic conditions (i.e. temperature

499   and rainfall) between Brittany and the Vosges Mountain (**Table 1**). The ~3 factor difference

500   between DSi in the Vosges and Brittany could be explained by the combined effect of the

501   groundwater temperature difference (~6°C) and precipitation difference (~1.5-fold). Indeed,

502   temperature affects weathering rates by one order of magnitude from 0 to 25°C (White and

503   Blum, 1995; White et al., 1999). This increase is further emphasized by increasing recharge

504   fluxes, which is related to rainfall conditions. Another effect which could explain the

505   difference for the mountainous catchment is lack of anthropogenic pressure related to

506   agriculture. Brittany is a region of intensive agriculture characterized by high nitrogen loads,

507   which induce soil acidification. High weathering rates have been observed related to fertilized

508   additions (Aquilina et al., 2012a) which may also partially explain the Vosges-Brittany

509   difference. Anyway, climatic and anthropogenic influences are not exclusive and may be

510   combined to explain the high weathering rate difference.

511   *5.2.3   Effect of groundwater abstraction on the weathering rate*

512   The weathering law for heavily-pumped catchment in Plœmeur (orange line, **Figure 9**)

513   displayed a substantially higher weathering rate (0.31 mg L^{-1} yr^{-1}) compared to the average

514   Brittany weathering rate (0.22 mg L^{-1} yr^{-1}). This might be due to the presence of CFC

515   contamination leading to artificially enriched CFC concentrations compared to their actual

516   residence times. The pumped catchment is indeed especially vulnerable to CFC

517   contaminations (**Table 1**). However, long-term monitoring of CFC and SF$_6$ and ^{3}H/^{3}He

518   measurements in this site makes the contamination hypothesis unlikely (Tarits et al., 2006).

519   The difference is more likely explained by the facts that: *i)* high and long-term pumping has

520   mobilized older waters (>100 years), which increase DSi concentrations without substantially

521   altering CFC concentrations (only dilution effect) (**Figure 4**); *ii)* pumping leads to a renewal

522   of groundwater flow paths with more reactive surfaces, leading to an increase of the reactive

523   surface/groundwater ratio.

524   **5.3   Use of DSi for inferring residence times in the unsaturated zone**

525   We hypothesized that the differences in initial DSi concentration are due to residence

526   time in the unsaturated zone, suggesting that DSi concentration at the groundwater table

527   surface (or modeled intercepts) could be used to infer residence times in the unsaturated zone.

528   Indeed the variability in C_{Si}^0 observed in **Table 2** is correlated with the average unsaturated

529   zone thickness (**Table 1**), a major, though not exclusive, control on the time spent in the

530   unsaturated zone (**Figure 10**). The high C_{Si}^0 for the pumped catchment (5.0 mg L^{-1}) could be

531   due to pumping-induced drawdown of the water table, which significantly increases the

532   unsaturated zone thickness. Likewise, the mountainous catchment has a much shallower water

533   table depth, which might be related to the low initial DSi concentration (2.9 mg L^{-1}). DSi

534   could therefore be a tracer of the full residence time in both unsaturated and saturated zones.

535   Yet, unless weathering rates in the unsaturated zone can be constrained, DSi estimates would

536   remain qualitative. Through tracing experiments, Legout et al. (2007) estimated the residence

537   time in the mobile-compartment of the unsaturated zone of the Kerrien catchment (South

538   Brittany) as 2-3 m y^{-1}, which induces weathering rates about 4 times higher than in the

539   saturated zone. However, the ratio mobile/immobile water is unknown but may represent a

540   large fraction of groundwater with long residence-time that may contribute to high DSi.

541   Because the unsaturated zone, including the base of the soil profile, is often the site of

542   elevated rates of biogeochemical activity (e.g. nitrogen retention and removal) (Legout et al.,

543   2005) or storage, constraining the residence time of water and solutes in this zone would

544   allow better estimation of catchment and regional-scale resilience to nutrient loading and

545   overall ecological functioning (Abbott et al., 2016; Meter et al., 2016; Pinay et al., 2015).
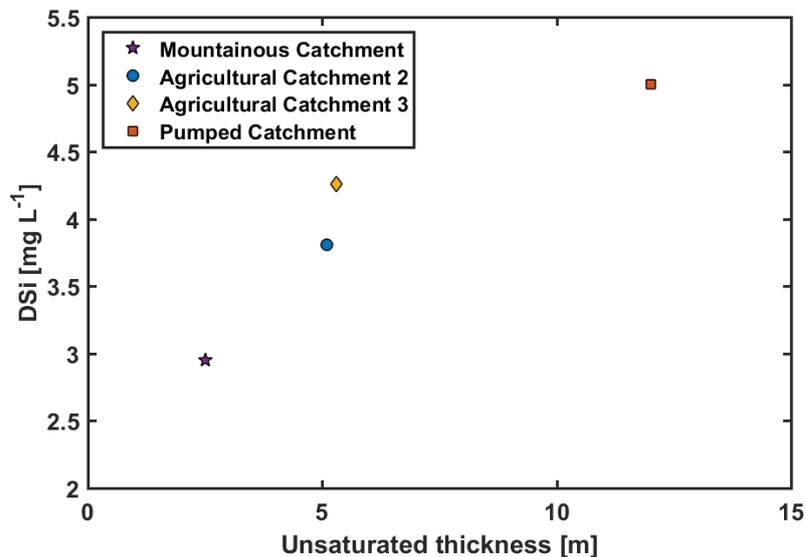
546

547   **Figure 10**: Initial DSi concentrations versus the average unsaturated zone thickness. The average

548   unsaturated zone thickness of the agricultural catchment 1 was not available.

549   **5.4   Comparison of weathering rates to previously estimated weathering rates**

550   We compared the weathering rates obtained in this study with previously published

551   studies (**Table 3**). The catchments considered in these studies have crystalline or sedimentary

552   bedrocks derived from the erosion of crystalline formations. Apparent weathering rates have

553   been estimated by different methods, either by implementing the geochemical evolution of

554   groundwater through advanced reactive transport modeling (Burns et al., 2003; Rademacher

555   et al., 2001) or by directly comparing DSi concentrations with apparent ages derived from

556   atmospheric tracer data (Bohlke and Denver, 1995; Clune and Denver, 2012; Denver et al.,

557   2010). Our methodology is intermediary as it combines lumped residence time distributions

558   with apparent weathering rates and inlet concentrations (atmospheric chronicles for CFCs and

559   initial concentration C_{Si}^{0} for DSi).

560   Except for the data reported in Kenoyer and Bowser (1992), which consists of young

561   groundwater (0-4 yrs), all DSi weathering rates referred in Table 3 are within one order of

562   magnitude (0.1 to 1 mg L^{-1} yr^{-1}). For catchments with apparent ages between 10 and 50 years,

563   weathering rates are clustered between 0.2 and 0.4 mg L^{-1} yr^{-1} (Figure 11), which is consistent

564   with weathering rates estimated in this study.

565   The initial decrease of weathering rates with the typical apparent ages might suggest a

566   power law dependence of weathering rates on groundwater age (Figure 11). However, for

567   older apparent ages, the weathering rates might also stabilize around 20 years (Figure 11,

568   insert) suggesting a transition from transport-limited to thermodynamically-limited conditions

569   consistent with what has been observed for feldspar minerals (Maher, 2010) with a slightly

570   older transition time (20 years here instead of 10 years). It will require more studies on this

571   residence time range (0-100 yrs) to decide between these two competing hypotheses (power

572   law dependence versus stabilization) and precisely locate the transition time (Ackerer et al.,

573   2018). This could be investigated by systematically combining weathering studies with

574   groundwater age tracer analysis in a diversity of environmental observatories. If predictable

575   rates are not found, the use of a constant weathering rate (equation (1)) could be refined by

576   considering a first order kinetic reaction, although it would require the inference of an

577   additional parameter to describe weathering.

578
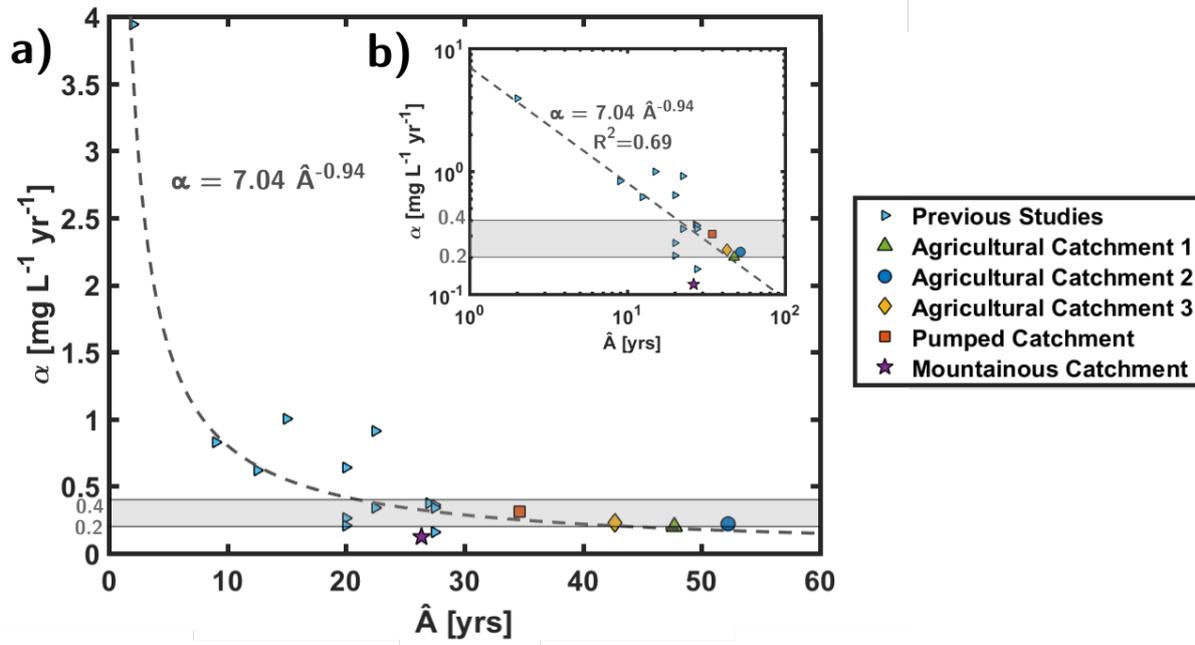
579

580   Figure 11: Silicate weathering rates α against the typical apparent age range $\hat{A}$ from which they have been

581   obtained, in this study and in previous studies (insert: log-log representation, p-value of $2 \cdot 10^{-5}$ obtained for

582   the fit).

Catchment	α [mg L^{-1} yr^{-1}]	Geological Context	Apparent Age range	Complementary information	References
Chesterville Branch	0.34	Permeable sand and gravel units of the fluvial Pensauken Formation and the marine glauconitic Aquia Formation.	5 – 40 yrs	Part of Locust Grove Catchment	(Bohlke and Denver, 1995)
Morgan Creek Drainage	0.37	Permeable sand and gravel units of the fluvial Pensauken Formation and the marine glauconitic Aquia Formation.	4 – 50 yrs	Part of Locust Grove Catchment	(Bohlke and Denver, 1995)
Panola Mountain Research Watershed	0.62	Panola Granite (granodiorite composition), a biotite–oligioclase– quartz– microcline granite of Mississippian to Pennsylvanian age.	0 – 25 yrs	Mainly Riparian Saprolite Aquifer	(Burns et al., 2003)
Bucks Branch Watershed	0.91	Sediments of the Beaverdam Formation.	15 – 30 yrs	mainly fluvial and estuarine deposits of sand, gravel, silt, and clays	(Clune and Denver, 2012)
Fairmount catchment	0.26	Permeable quartz sand and gravel of the Beaverdam Formation and underlying sandy strata of the Bethany Formation.	5 – 35 yrs	well-drained settings with relatively deep water tables and thick sandy aquifers	(Denver et al., 2010)
Locust Grove catchment	0.16	Permeable quartz sand and gravel of the Pennsauken Formation underlain by highly weathered glauconitic sands of the Aquia Formation.	5 – 50 yrs	well-drained settings with relatively deep water tables and thick sandy aquifers	(Denver et al., 2010)
Lizzie Catchment	0.36	Several Pleistocene-age terrace deposits that are underlain by a confining unit on the top of the Yorktown Formation.	5 – 50 yrs	predominantly poorly drained settings with shallow water tables	(Denver et al., 2010)
Willards Catchment	0.83	The lowermost unit of the system is the Beaverdam Sand, which is overlain by a 3 to 8 m thick layer of clay, silt, peat, and sand of the Omar Formation.	0 – 18 yrs	predominantly poorly drained settings with shallow water tables	(Denver et al., 2010)
Polecat Creek Watershed	1.0	Piedmont crystalline coastal plain sediments and alluvium. Presence of Saprolite.	0 – 30 yrs	Bedrock garnet-biotite gneiss	(Lindsey et al., 2003)
Crystal Lake, Vilas County (Wisconsin)	3.94	50 m of glacial sediment which overlies Precambrian bedrock.	0 – 4 yrs	Glacial sediments were eroded from Precambrian bedrock lithologies	(Kenoyer and Bowser, 1992)
Sagehen Springs (CA).	0.17 – 1.11	Extensive glacial till deposits derived from a combination of andesite and granodiorite basement rocks. The granodiorite consists primarily of plagioclase (40%), quartz (30%), hornblende (20%), and biotite (10%), and the andesite consists primarily of plagioclase (45%) with varying amounts of hornblende (5–25%) and augite (1–25%) and a small amount of glassy groundmass.	0 – 40 yrs	Range of weathering rate determined for each spring, **only for plagioclase mineral.**	(Rademacher et al., 2001)
Sagehen Springs (CA).	0.06 - 0.35		0 – 40 yrs	Range of weathering rate determined for each spring, **only for hornblende mineral.**	(Rademacher et al., 2001)
Lizzie Catchment	0.34	Several Pleistocene-age terrace deposits that are underlain by a confining unit on the top of the Yorktown Formation.	5 – 50 yrs	Unconfined aquifer.	(Tesoriero et al., 2005)

584   **Table 3**: Published weathering rates in different catchments obtained either directly or by fitting DSi concentrations against apparent ages. The typical age range

585   gives the spread of the water age data obtained from the different sampled wells.

6   Conclusion

We investigated the relationship between DSi and groundwater age tracers (CFCs) in five different crystalline catchments, including lowland, mountainous, and actively pumped catchments. For each catchment, we quantified the weathering rate and the RTDs at multiple wells using inverse Gaussian lumped parameter models calibrated with geochemical data. Overall, the DSi was strongly related to the exposure time between rocks and recently recharged groundwater (i.e. between 5 to 100 years). We found that DSi was highly complementary to CFCs, allowing better quantification of RTDs, including in the unsaturated zone and for water masses younger and older than the now rapidly closing CFC use's window. The consistency of DSi weathering rates in three Brittany catchments suggests that DSi may be a robust and cheap groundwater age proxy at regional scales for catchments with comparable geology and climate. We interpreted DSi accumulation differences in the Brittany pumped site and the mountainous region, as a consequence of temperature differences and alterations of flow from groundwater abstraction respectively. If the temperature sensitivity of weathering can be constrained, this tracer could allow widespread determination of water transit time at the catchment scale for the unsaturated zone, aquifer, and surface waters.

References

609

610 Abbott BW, Baranov V, Mendoza-Lera C, Nikolakopoulou M, Harjung A, Kolbe T, et al., 2016.
611   Using multi-tracer inference to move beyond single-catchment ecohydrology. Earth-Science
612   Reviews. 160, 19-42. http://dx.doi.org/10.1016/j.earscirev.2016.06.014.

613 Abbott BW, Moatar F, Gauthier O, Fovet O, Antoine V, Ragueneau O, 2018. Trends and seasonality
614   of river nutrients in agricultural catchments: 18years of weekly citizen science in France.
615   Science of The Total Environment. 624, 845-858.
616   https://doi.org/10.1016/j.scitotenv.2017.12.176.

617 Ackerer J, Chabaux F, Lucas Y, Clément A, Fritz B, Beaulieu E, et al., 2018. Monitoring and reactive-
618   transport modeling of the spatial and temporal variations of the Strengbach spring
619   hydrochemistry. Geochimica et Cosmochimica Acta. 225, 17-35.
620   https://doi.org/10.1016/j.gca.2018.01.025.

621 Anderson RS, Anderson SP, 2010. Geomorphology: the mechanics and chemistry of landscapes:
622   Cambridge University Press.

623 Anderson SP, Dietrich WE, Brimhall GH, 2002. Weathering profiles, mass-balance analysis, and rates
624   of solute loss: Linkages between weathering and erosion in a small, steep catchment.
625   Geological Society of America Bulletin. 114, 1143-1158.

626 Appelo C, Postma D, 1994. Geochemistry, Groundwater and Pollution: AA Balkema, Brookfield.

627 Aquilina L, Poszwa A, Walter C, Vergnaud V, Pierson-Wickmann A-C, Ruiz L, 2012a. Long-Term
628   Effects of High Nitrogen Loads on Cation and Carbon Riverine Export in Agricultural
629   Catchments. Environmental Science & Technology. 46, 9447-9455. 10.1021/es301715t.

630 Aquilina L, Vergnaud-Ayraud V, Labasque T, Bour O, Molenat J, Ruiz L, et al., 2012b. Nitrate
631   dynamics in agricultural catchments deduced from groundwater dating and long-term nitrate
632   monitoring in surface- and groundwaters. Science of the Total Environment. 435, 167-178.
633   10.1016/j.scitotenv.2012.06.028.

634 Aubert D, Stille P, Probst A, 2001. REE fractionation during granite weathering and removal by
635   waters and suspended loads: Sr and Nd isotopic evidence. Geochimica et Cosmochimica Acta.
636   65, 387-406. http://dx.doi.org/10.1016/S0016-7037(00)00546-9.

637 Ayraud V, 2005. Détermination du temps de résidence des eaux souterraines: application au transfert
638   d'azote dans les aquifères fracturés hétérogènes. Université Rennes 1

639 Ayraud V, Aquilina L, Labasque T, Pauwels H, Molenat J, Pierson-Wickmann A-C, et al., 2008.
640   Compartmentalization of physical and chemical properties in hard-rock aquifers deduced from
641   chemical and groundwater age analyses. Applied Geochemistry. 23, 2686-2707.
642   https://doi.org/10.1016/j.apgeochem.2008.06.001.

643 Becker SK, 2013. Assessing the Use of Dissolved Silicon as a Proxy for Groundwater Age: A Critical
644   Analysis of Published Data and New Data from the North Carolina Coastal Plain. MSc

645 Beyer M, Jackson B, Daughney C, Morgenstern U, Norton K, 2016. Use of hydrochemistry as a
646   standalone and complementary groundwater age tracer. Journal of Hydrology. 543, 127-144.
647   10.1016/j.jhydrol.2016.05.062.

648 Bochet O, 2017. Caractérisation des hot spots de réactivité biogéochimique dans les eaux souterraines.
649   Rennes 1

650 Bochet O, Bethencourt L, Dufresne A, Pedrot M, Farasin J, Labasque T, et al., under revision.
651   Dynamic microbiological hot spots sustained by mixing in subsurface fractures. Nature
652   Geosci.

653 Bohlke JK, Denver JM, 1995. Combined use of groundwater dating, chemical, and isotopic analyses
654   to resolve the history and fate of nitrate contamination in 2 agricultural watersheds, atlantic
655   coastal-plain, maryland. Water Resources Research. 31, 2319-2339. 10.1029/95wr01584.

656 Bouhnik-Le Coz M, Petitjean P, Serrat E, Gruau G, 2001. Validation d'un protocole permettant le
657   dosage simultané des cations majeurs et traces dans les eaux douces naturelles par ICP-MS

658 Bouraoui F, Grizzetti B, 2011. Long term change of nutrient concentrations of rivers discharging in
659   European seas. Science of The Total Environment. 409, 4899-4916.
660   http://dx.doi.org/10.1016/j.scitotenv.2011.08.015.

661 Burns DA, Plummer LN, McDonnell JJ, Busenberg E, Casile GC, Kendall C, et al., 2003. The
662   Geochemical Evolution of Riparian Ground Water in a Forested Piedmont Catchment. Ground
663   Water. 41, 913-925. 10.1111/j.1745-6584.2003.tb02434.x.

664 Busenberg E, Plummer LN, 1992. Use of chlorofluorocarbons (CCl3F and CCl2F2) as hydrologic
665   tracers and age-dating tools: The alluvium and terrace system of central Oklahoma. Water
666   Resources Research. 28, 2257-2283. 10.1029/92WR01263.

667 Chabaux F, Viville D, Lucas Y, Ackerer J, Ranchoux C, Bosia C, et al., 2017. Geochemical tracing
668   and modeling of surface and deep water–rock interactions in elementary granitic watersheds
669   (Strengbach and Ringelbach CZOs, France). Acta Geochimica. 36, 363-366. 10.1007/s11631-
670   017-0163-5.

671 Clune JW, Denver JM, 2012. Residence Time, Chemical and Isotopic Analysis of Nitrate in the
672   Groundwater and Surface Water of a Small Agricultural Watershed in the Coastal Plain,
673   Bucks Branch, Sussex County, Delaware: US Department of the Interior, US Geological
674   Survey.

675 Cook PG, Herczeg AL, 2000. Environmental Tracers in Subsurface Hydrology: Springer.

676 De Dreuzy J-R, Bodin J, Le Grand H, Davy P, Boulanger D, Battais A, et al., 2006. General Database
677   for Ground Water Site Information. Ground Water. 44, 743-748. 10.1111/j.1745-
678   6584.2006.00220.x.

679 Delvaux C, Cardinal D, Carbonnel V, Chou L, Hughes HJ, André L, 2013. Controls on riverine $\delta 30Si$
680   signatures in a temperate watershed under high anthropogenic pressure (Scheldt — Belgium).
681   Journal of Marine Systems. 128, 40-51. https://doi.org/10.1016/j.jmarsys.2013.01.004.

682 Denver JM, Tesoriero AJ, Barbaro JR, 2010. Trends and Transformation of Nutrients and Pesticides in
683   a Coastal Plain Aquifer System, United States All rights reserved. No part of this periodical
684   may be reproduced or transmitted in any form or by any means, electronic or mechanical,
685   including photocopying, recording, or any information storage and retrieval system, without
686   permission in writing from the publisher. Journal of Environmental Quality. 39, 154-167.
687   10.2134/jeq2009.0107.

688 Eberts SM, Bohlke JK, Kauffman LJ, Jurgens BC, 2012. Comparison of particle-tracking and lumped-
689   parameter age-distribution models for evaluating vulnerability of production wells to
690   contamination. Hydrogeology Journal. 20, 263-282. 10.1007/s10040-011-0810-6.

691 Edmunds WM, Smedley PL, 2000. Residence time indicators in groundwater: the East Midlands
692   Triassic sandstone aquifer. Applied Geochemistry. 15, 737-752.
693   http://dx.doi.org/10.1016/S0883-2927(99)00079-7.

694 Galloway JN, Townsend AR, Erisman JW, Bekunda M, Cai Z, Freney JR, et al., 2008. Transformation
695   of the Nitrogen Cycle: Recent Trends, Questions, and Potential Solutions. Science. 320, 889-
696   892. 10.1126/science.1136674.

697 Gelhar LW, Axness CL, 1983. Three-dimensional stochastic analysis of macrodispersion in aquifers.
698   Water Resources Research. 19, 161-180.

699   Green CT, Zhang Y, Jurgens BC, Starn JJ, Landon MK, 2014. Accuracy of travel time distribution
700   (TTD) models as affected by TTD complexity, observation errors, and model and tracer
701   selection. Water Resources Research, 6191 - 6213. 10.1002/2014WR015625.

702   Haggerty R, Gorelick SM, 1995. Multiple-rate mass transfer for modeling diffusion and surface
703   reactions in media with pore-scale heterogeneity. Water Resources Research. 31, 2383-2400.
704   10.1029/95WR10583.

705   Haitjema HM, 1995. Analytic element modeling of groundwater flow: Academic press.

706   Hughes HJ, Sondag F, Santos RV, André L, Cardinal D, 2013. The riverine silicon isotope
707   composition of the Amazon Basin. Geochimica et Cosmochimica Acta. 121, 637-651.
708   https://doi.org/10.1016/j.gca.2013.07.040.

709   Iler RK, 1979. The chemistry of silica: solubility, polymerization, colloid and surface properties, and
710   biochemistry. . Canada: John Wiley &Sons Inc

711   Ingber L, 2000. Adaptive simulated annealing (ASA): Lessons learned. eprint arXiv:cs/0001018

712   Jarvie HP, Sharpley, A.N., Withers, P.J.A., Scott, J.T., Haggard, B.E., Neal, C., 2013. Phosphorus
713   Mitigation to Control River Eutrophication: Murky Waters, Inconvenient Truths, and
714   "Postnormal" Science. J. Environ. Qual. . 42, 295-304. 10.2134/jeq2012.0085.

715   Jasechko S, Perrone D, Befus KM, Bayani Cardenas M, Ferguson G, Gleeson T, et al., 2017. Global
716   aquifers dominated by fossil groundwaters but wells vulnerable to modern contamination.
717   Nature Geosci. 10, 425-429. 10.1038/ngeo2943.

718   Jenny J-P, Normandeau A, Francus P, Taranu ZE, Gregory-Eaves I, Lapointe F, et al., 2016. Urban
719   point sources of nutrients were the leading cause for the historical spread of hypoxia across
720   European lakes. Proceedings of the National Academy of Sciences. 113, 12655-12660.
721   10.1073/pnas.1605480113.

722   Jiménez-Martínez J, Longuevergne L, Le Borgne T, Davy P, Russian A, Bour O, 2013. Temporal and
723   spatial scaling of hydraulic response to recharge in fractured aquifers: Insights from a
724   frequency domain analysis. Water Resources Research. 49, 3007-3023. 10.1002/wrcr.20260.

725   Jurgens BC, Böhlke JK, Eberts SM, 2012. TracerLPM (Version 1): An Excel® workbook for
726   interpreting groundwater age distributions from environmental tracer data. U.S. Geological
727   Survey Techniques and Methods Report, 60.

728   Kenoyer GJ, Bowser CJ, 1992. Groundwater chemical evolution in a sandy silicate aquifer in northern
729   Wisconsin: 1. Patterns and rates of change. Water Resources Research. 28, 579-589.
730   10.1029/91WR02302.

731   Kim K, 2002. Plagioclase weathering in the groundwater system of a sandy, silicate aquifer.
732   Hydrological Processes. 16, 1793-1806. doi:10.1002/hyp.1081.

733   Kolbe T, Marçais J, Thomas Z, Abbott BW, de Dreuzy J-R, Rousseau-Gueutin P, et al., 2016.
734   Coupling 3D groundwater modeling with CFC-based age dating to classify local groundwater
735   circulation   in   an   unconfined   crystalline   aquifer.   Journal   of
736   Hydrologyhttp://dx.doi.org/10.1016/j.jhydrol.2016.05.020.

737   Labasque T, Aquilina L, Vergnaud V, Barbecot F, 2014. Inter-laboratory comparison of the analyses
738   of sulphur hexafluoride (SF6) and three chlorofluorocarbons (CFC-11, -12 and -113) in
739   groundwater   and   an   air   standard.   Applied   Geochemistry.   50,   118-129.
740   http://dx.doi.org/10.1016/j.apgeochem.2014.03.009.

741   Labasque T, Ayraud V, Aquilina L, Le Corre P, 2006. Dosage des composés chlorofluorocarbonés et
742   du tétrachlorure de carbone dans les eaux souterraines: application à la datation des eaux.
743   Cahiers Techniques de Géosciences Rennes. 4

744 Le Borgne T, Bour O, Paillet FL, Caudal JP, 2006. Assessment of preferential flow path connectivity
745   and hydraulic properties at single-borehole and cross-borehole scales in a fractured aquifer.
746   Journal of Hydrology. 328, 347-359.

747 Legout C, Molenat J, Aquilina L, Gascuel-Odoux C, Faucheux M, Fauvel Y, et al., 2007. Solute
748   transfer in the unsaturated zone-groundwater continuum of a headwater catchment. Journal of
749   Hydrology. 332, 427-441. http://dx.doi.org/10.1016/j.jhydrol.2006.07.017.

750 Legout C, Molenat J, Lefebvre S, Marmonier P, Aquilina L, 2005. Investigation of biogeochemical
751   activities in the soil and unsaturated zone of weathered granite. Biogeochemistry. 75, 329-350.
752   10.1007/s10533-005-0110-0.

753 Leray S, de Dreuzy J-R, Bour O, Aquilina L, Labasque T, 2012. Contribution of age data to the
754   characterization of complex aquifers. Journal of Hydrology, 54-68.

755 Leray S, Engdahl NB, Massoudieh A, Bresciani E, McCallum J, 2016. Residence time distributions
756   for hydrologic systems: Mechanistic foundations and steady-state analytical solutions. Journal
757   of Hydrologyhttp://dx.doi.org/10.1016/j.jhydrol.2016.01.068.

758 Lindsey BD, Phillips SW, Donnelly CA, Speiran GK, Plummer LN, Böhlke J-K, et al., 2003.
759   Residence times and nitrate transport in ground water discharging to streams in the
760   Chesapeake Bay Watershed. US Geological Survey Water-Resources Investigations Report. 3,
761   4035.

762 Lucas Y, Chabaux F, Schaffhauser T, Fritz B, Ambroise B, Ackerer J, et al., 2017. Hydrogeochemical
763   modeling (KIRMAT) of spring and deep borehole water compositions in the small granitic
764   Ringelbach catchment (Vosges Mountains, France). Applied Geochemistry. 87, 1-21.
765   https://doi.org/10.1016/j.apgeochem.2017.10.005.

766 Maher K, 2010. The dependence of chemical weathering rates on fluid residence time. Earth and
767   Planetary Science Letters. 294, 101-110. http://dx.doi.org/10.1016/j.epsl.2010.03.010.

768 Maher K, 2011. The role of fluid residence time and topographic scales in determining chemical
769   fluxes   from   landscapes.   Earth   and   Planetary   Science   Letters.   312,   48-58.
770   http://dx.doi.org/10.1016/j.epsl.2011.09.040.

771 Maher K, Druhan J, 2014. Relationships between the Transit Time of Water and the Fluxes of
772   Weathered Elements through the Critical Zone. Procedia Earth and Planetary Science. 10, 16-
773   22. https://doi.org/10.1016/j.proeps.2014.08.004.

774 Maloszewski P, Zuber A, 1996. Lumped   parameter   models   for   the   interpretation   of
775   environmentaltracer data. In: Manual On Mathematical Models in Isotope Hydrology. Vienna,
776   Austria, IAEA-TECDOC. 910, 9–58.

777 Marçais J, de Dreuzy JR, Ginn TR, Rousseau-Gueutin P, Leray S, 2015. Inferring transit time
778   distributions from atmospheric tracer data: Assessment of the predictive capacities of Lumped
779   Parameter Models on a 3D crystalline aquifer model. Journal of Hydrology. 525, 619-631.
780   http://dx.doi.org/10.1016/j.jhydrol.2015.03.055.

781 Meter KJV, Basu NB, 2017. Time lags in watershed-scale nutrient transport: an exploration of
782   dominant controls. Environmental Research Letters. 12, 084017. https://doi.org/10.1088/1748-
783   9326/aa7bf4.

784 Meter KJV, Basu NB, Veenstra JJ, Burras CL, 2016. The nitrogen legacy: emerging evidence of
785   nitrogen accumulation in anthropogenic landscapes. Environmental Research Letters. 11,
786   035014. https://doi.org/10.1088/1748-9326/11/3/035014.

787 Morgenstern U, Daughney CJ, Leonard G, Gordon D, Donath FM, Reeves R, 2015. Using
788   groundwater age and hydrochemistry to understand sources and dynamics of nutrient
789   contamination through the catchment into Lake Rotorua, New Zealand. Hydrology and Earth
790   System Sciences. 19, 803-822. 10.5194/hess-19-803-2015.

791   Morgenstern U, Stewart MK, Stenger R, 2010. Dating of streamwater using tritium in a post nuclear
792   bomb pulse world: continuous variation of mean transit time with streamflow. Hydrol. Earth
793   Syst. Sci. 14, 2289-2301. 10.5194/hess-14-2289-2010.

794   Peters NE, Burns DA, Aulenbach BT, 2014. Evaluation of High-Frequency Mean Streamwater
795   Transit-Time Estimates Using Groundwater Age and Dissolved Silica Concentrations in a
796   Small Forested Watershed. Aquatic Geochemistry. 20, 183-202. 10.1007/s10498-013-9207-6.

797   Pfister L, Wetzel CE, Klaus J, Martínez-Carreras N, Antonelli M, Teuling AJ, et al., 2017. Terrestrial
798   diatoms as tracers in catchment hydrology: a review. Wiley Interdisciplinary Reviews: Water.
799   4, e1241. doi:10.1002/wat2.1241.

800   Pierret MC, Stille P, Prunier J, Viville D, Chabaux F, 2014. Chemical and U–Sr isotopic variations in
801   stream and source waters of the Strengbach watershed (Vosges mountains, France). Hydrol.
802   Earth Syst. Sci. 18, 3969-3985. 10.5194/hess-18-3969-2014.

803   Pinay G, Peiffer S, De Dreuzy J-R, Krause S, Hannah D, Fleckenstein J, et al., 2015. Upscaling
804   Nitrogen Removal Capacity from Local Hotspots to Low Stream Orders' Drainage Basins.
805   Ecosystems, 1-20. 10.1007/s10021-015-9878-5.

806   Rademacher LK, Clark JF, Hudson GB, Erman DC, Erman NA, 2001. Chemical evolution of shallow
807   groundwater as recorded by springs, Sagehen basin; Nevada County, California. Chemical
808   Geology. 179, 37-51. https://doi.org/10.1016/S0009-2541(01)00314-X.

809   Rockstrom J, Steffen W, Noone K, Persson A, Chapin FS, III, Lambin EF, et al., 2009. A safe
810   operating space for humanity. Nature. 461, 472-475. 10.1038/461472a.

811   Roques C, Aquilina L, Bour O, Maréchal J-C, Dewandel B, Pauwels H, et al., 2014a. Groundwater
812   sources and geochemical processes in a crystalline fault aquifer. Journal of Hydrology. 519,
813   Part D, 3110-3128. http://dx.doi.org/10.1016/j.jhydrol.2014.10.052.

814   Roques C, Bour O, Aquilina L, Dewandel B, Leray S, Schroetter JM, et al., 2014b. Hydrological
815   behavior of a deep sub-vertical fault in crystalline basement and relationships with
816   surrounding   reservoirs.   Journal   of   Hydrology.   509,   42-54.
817   http://dx.doi.org/10.1016/j.jhydrol.2013.11.023.

818   Sebilo M, Mayer B, Nicolardot B, Pinay G, Mariotti A, 2013. Long-term fate of nitrate fertilizer in
819   agricultural soils. Proceedings of the National Academy of Sciences of the United States of
820   America. 110, 18185-18189. 10.1073/pnas.1305372110.

821   Singleton MJ, Esser BK, Moran JE, Hudson GB, McNab WW, Harter T, 2007. Saturated Zone
822   Denitrification: Potential for Natural Attenuation of Nitrate Contamination in Shallow
823   Groundwater Under Dairy Operations. Environmental Science & Technology. 41, 759-765.
824   10.1021/es061253g.

825   Spalding RF, Exner ME, 1993. Occurrence of nitrate in groundwater - a review. Journal of
826   Environmental Quality. 22, 392-402. 10.2134/jeq1993.00472425002200030002x.

827   Steffen W, Richardson K, Rockström J, Cornell SE, Fetzer I, Bennett EM, et al., 2015. Planetary
828   boundaries: Guiding   human   development   on   a   changing   planet.   Science.
829   34710.1126/science.1259855.

830   Stewart MK, Mehlhorn J, Elliott S, 2007. Hydrometric and natural tracer (oxygen-18, silica, tritium
831   and sulphur hexafluoride) evidence for a dominant groundwater contribution to Pukemanga
832   Stream, New Zealand. Hydrological Processes. 21, 3340-3356. doi:10.1002/hyp.6557.

833   Suckow A, 2014. The age of groundwater - Definitions, models and why we do not need this term.
834   Applied Geochemistry. 50, 222-230. 10.1016/j.apgeochem.2014.04.016.

835   Tarits C, Aquilina L, Ayraud V, Pauwels H, Davy P, Touchard F, et al., 2006. Oxido-reduction
836   sequence related to flux variations of groundwater from a fractured basement aquifer

837   (Ploemeur   area,   France).   Applied   Geochemistry.   21,   29-47.
838   https://doi.org/10.1016/j.apgeochem.2005.09.004.

839   Tesoriero AJ, Spruill TB, Mew HE, Farrell KM, Harden SL, 2005. Nitrogen transport and
840   transformations in a coastal plain watershed: Influence of geomorphology on flow paths and
841   residence times. Water Resources Research. 41, n/a-n/a. 10.1029/2003WR002953.

842   Thamatrakoln K, Hildebrand M, 2008. Silicon uptake in diatoms revisited: a model for saturable and
843   nonsaturable uptake kinetics and the role of silicon transporters. Plant Physiol. 146, 1397-407.
844   10.1104/pp.107.107094.

845   Thomas Z, Abbott BW, Troccaz O, Baudry J, Pinay G, 2016a. Proximate and ultimate controls on
846   carbon and nutrient dynamics of small agricultural catchments. Biogeosciences. 13, 1863-
847   1875. 10.5194/bg-13-1863-2016.

848   Thomas Z, Rousseau-Gueutin P, Kolbe T, Abbott BW, Marçais J, Peiffer S, et al., 2016b. Constitution
849   of a catchment virtual observatory for sharing flow and transport models outputs. Journal of
850   Hydrology. 543, 59-66. https://doi.org/10.1016/j.jhydrol.2016.04.067.

851   Touchard F, 1999. Caractérisation hydrogéologique d'un aquifère en socle fracturé. Site de Ploëmeur
852   (Morbihan).

853   Visser A, Broers HP, Purtschert R, Sultenfuss J, de Jonge M, 2013. Groundwater age distributions at a
854   public drinking water supply well field derived from multiple age tracers (Kr-85, H-3/He-3,
855   and Ar-39). Water Resources Research. 49, 7778-7796. 10.1002/2013wr014012.

856   Visser A, Fourré E, Barbecot F, Aquilina L, Labasque T, Vergnaud V, et al., 2014. Intercomparison of
857   tritium and noble gases analyses, 3H/3He ages and derived parameters excess air and recharge
858   temperature.   Applied   Geochemistry.   50,   130-141.
859   http://dx.doi.org/10.1016/j.apgeochem.2014.03.005.

860   Viville D, Chabaux F, Stille P, Pierret MC, Gangloff S, 2012. Erosion and weathering fluxes in
861   granitic basins: The example of the Strengbach catchment (Vosges massif, eastern France).
862   CATENA. 92, 122-129. http://dx.doi.org/10.1016/j.catena.2011.12.007.

863   White AF, 2008. Quantitative Approaches to Characterizing Natural Chemical Weathering Rates. In:
864   Brantley SL, Kubicki JD, White AF, editors. Kinetics of Water-Rock Interaction. Springer
865   New York, New York, NY, pp. 469-543.

866   White AF, Blum AE, 1995. Effects of climate on chemical weathering in watersheds. Geochimica et
867   Cosmochimica Acta. 59, 1729-1747. http://dx.doi.org/10.1016/0016-7037(95)00078-E.

868   White AF, Blum AE, Bullen TD, Vivit DV, Schulz M, Fitzpatrick J, 1999. The effect of temperature
869   on experimental and natural chemical weathering rates of granitoid rocks. Geochimica et
870   Cosmochimica Acta. 63, 3277-3291. http://dx.doi.org/10.1016/S0016-7037(99)00250-1.

871   White AF, Brantley SL, 2003. The effect of time on the weathering of silicate minerals: why do
872   weathering rates differ in the laboratory and field? Chemical Geology. 202, 479-506.
873   http://dx.doi.org/10.1016/j.chemgeo.2003.03.001.

874   White AF, Bullen TD, Schulz MS, Blum AE, Huntington TG, Peters NE, 2001. Differential rates of
875   feldspar weathering in granitic regoliths. Geochimica et Cosmochimica Acta. 65, 847-869.
876   http://dx.doi.org/10.1016/S0016-7037(00)00577-9.

877   Wilcock RJ, Monaghan RM, Quinn JM, Srinivasan MS, Houlbrooke DJ, Duncan MJ, et al., 2013.
878   Trends in water quality of five dairy farming streams in response to adoption of best practice
879   and benefits of long-term monitoring at the catchment scale. Marine and Freshwater Research.
880   64, 401-412. https://doi.org/10.1071/MF12155.

881